

FINAL REPORT

U.S. Department of Energy

Permanganate Treatment of DNAPLs in Reactive Barriers and Source Zone Flooding
Schemes

Principal Investigator and Institution:
Dr. Franklin W. Schwartz
Department of Geological Sciences
The Ohio State University
Columbus, OH

Project Number: 73745
Grant Number: DE-FG07-00ER15115

Grant Project Officers:
Contract Specialist; Dallas Hoffer,
Technical Program Officers; Roland F. Hirsch, Beth A. Moore

Project Duration: 9/15/2000-9/14/2003

December, 2003

TABLE OF CONTENTS

PROJECT OBJECTIVES AND SUMMARY	3
METHODS AND RESULTS	4
1. <i>A Review of In-Situ Chemical Oxidation and Heterogeneity</i>	4
2. <i>Increasing DNAPL Removal Rate Through Treatment of Mn Oxide Precipitates</i>	9
3. <i>Destruction Efficiencies and Dynamics of Reaction Fronts</i>	15
4. <i>Computer Model Development</i>	21
RELEVANCE, IMPACT AND TECHNOLOGY TRANSFER	33
PROJECT PRODUCTIVITY	33
PERSONNEL SUPPORTED	33
PUBLICATIONS	34
INTERACTIONS	34
LITERATURE CITED	36

PROJECT OBJECTIVES AND SUMMARY

This research involves a combined experimental modeling study that builds on our previous DOE-sponsored work in understanding how KMnO_4 can be used with in situ cleanups of contaminated sites. The specific objectives of this study are (1) to describe how solid forms of KMnO_4 behave in saturated media, (2) to undertake flow tank studies that examine the hydraulic impact of reaction products (especially MnO_2) on the flux of water through the zone of contamination, and (3) to represent process understanding in flow and transport models.

We have made excellent progress in addressing these issues through a variety of different laboratory and theoretical investigations, as well as work that summarizes the state of the science. In the space available for this report, we can only summarize the key findings of the study. Readers interested in additional details can refer to the papers that are listed at end of this report.

There has been significant industrial interest in the use of KMnO_4 schemes for the in situ destruction of various chlorinated solvents. Given our previous work that emphasized some of the problems associated with field applications of the method, we were invited to contribute to a special edition of *Environmental & Engineering Geoscience* that examined the effects of heterogeneity on in situ remediation schemes. Our review targeted the most common implementation namely the use of an injection/withdrawal system to circulate oxidants (e.g., potassium permanganate, hydrogen peroxide, and Fenton's Reagent) through a source zone containing a dense nonaqueous phase liquid (DNAPL). The review demonstrated with various examples (i) how the efficiency of chemical oxidation is highly dependent on physical and chemical heterogeneities, and (ii) how effective delivery is essential for successful remediation. A summary of this work is provided here in Section 1 of the Chapter Methods and Results.

We investigated the mineralogy of Mn oxides, and the possibilities of controlling the colloid growth and removing the solid precipitates by dissolution. We determined the chemical formula of the Mn oxide and identified as semi-amorphous potassium-rich birnessite. We also measured the surface properties of the Mn oxide like the specific surface area and point of zero charge (pzc) of the Mn oxide. These findings provide foundation for further investigation of the behavior of Mn oxide precipitates in the remediation environment. We utilized batch experiments to explore the feasibility of applying phosphate to slow down the formation of colloidal Mn oxide. Our results show that phosphate can slow down the formation of the colloids, especially early in the reaction. A model was proposed to describe the reaction process. Our study provides scientific background on the possibility to slow down the formation of colloid during the oxidation scheme by chemical additives. The dissolution kinetics of Mn oxide was evaluated in batch experiments using solutions of citric acid, oxalic acid, and EDTA. Organic acids dissolve Mn oxide quickly. Reaction rates increase with acid concentration, as tested with citric acid. The Mn oxide dissolution mechanism likely involves proton and ligand-promoted dissolution and reductive dissolution. We proposed two models describing the dissolution of Mn oxide by organic acids. The flow tank experiment confirmed the possibilities of restoring permeability damaged by Mn oxide precipitation. There seem to be good possibilities for using citrate and oxalate to control plugging

created by the precipitation of Mn oxide. A more details summary of the work on the Mn oxide precipitates is provided here in Section 2 of the Chapter Methods and Results.

Another important thrust of our research effort involved a detailed evaluation of the efficiency of TCE removal with time, and the space/time dynamics of the solid-phase oxidation reaction front (Section 3 of the Chapter Methods and Results). The approach involved a very large 3-D flow tank experiment. The progress of TCE destruction and the distribution of MnO₂ precipitates were monitored using novel optical and chemical monitoring techniques. The results showed that the efficiency of the KMnO₄ treatment of chlorinated solvents in the flushing scheme diminished with time due to the formation of low-permeability reaction zones in the TCE source and along the downstream edge of the TCE plume. In effect plugging caused relatively large quantities of unreacted KMnO₄ solution to by-pass the source zone during the flushing activity. Interestingly, a zone of precipitation along the sides of the dissolved plume reduced the mixing of the plume and potential oxidants. Overall, it was difficult for KMnO₄ to contact zones with NAPLs and dissolved-phase contaminants. These results support our suggestion that a development of a new KMnO₄ treatment scheme that could provide both contaminant destruction and plugging/permanganate control is required.

Over this study, work continued on the development of the ISCO3D computer code, which began with our previous of the previous EMSP grant. At the end of that study, a preliminary version of the code was operational (Zhang and Schwartz, 2000b). Early in the present study, we spent time in improving the input/output structure of the code to make it more user friendly, in documenting the verification and other test problems, and in developing a detailed user's guide for the code. These aspects led to the production of a 96 page User's Guide, which is discussed in more detail in Section 4 of the Chapter Methods and Results.

Significant progress was made in removing a significant limitation of the code, which was based on the assumption that porosity and permeability did not change as reaction products (solids, gases). This assumption is probably valid for problems in coarse porous media where DNAPL saturations are low. However, our experiments provided examples of situations where extensive plugging of the porous medium is evident. We modified the code (see Section 4 of the Chapter Methods and Results) to account for changes in permeability and porosity due to the reactants. At this time, additional work is underway to complete the analysis of preliminary simulation trials and to write a paper integrating modeling and experimental results.

METHODS AND RESULTS

1. A Review of In-Situ Chemical Oxidation and Heterogeneity

Chemical oxidants are increasingly being used for the in-situ destruction of organic contaminants in ground water. The most common implementation involves using an injection/withdrawal system to circulate oxidants (e.g., potassium permanganate, hydrogen peroxide, and Fenton's Reagent) through a source zone containing a dense non-aqueous phase liquid (DNAPL). Because the efficiency of chemical oxidation is highly

dependent on physical and chemical heterogeneities, effective delivery schemes are essential for successful remediation. This study reviews the impact of heterogeneities on the success of in-situ chemical oxidation.

Impact of Physical Heterogeneity

Physical heterogeneity is caused by variability in hydraulic conductivity. For a source-zone flooding scheme (permanganate, Fenton's, or ozone) to be successful, a large mass of the oxidizing fluid needs to be delivered. However, in most cases, the mass of oxidant consumed by the target compound is small compared to the background demand. Thus, the combination of competitive consumption of the oxidant by other substances and a low hydraulic conductivity can severely limit the quantity of contaminant transformed. Ozone sparging systems also are influenced by hydraulic conductivity distributions because gas-flow channels form in media with the greatest pore size, and by inference the highest permeability (Ahfeld et al., 1994). Channels carrying ozone will be diverted around lower permeability units.

Also, when DNAPL saturations are high in a permeable unit, the relative permeability of that zone for a treatment chemical dissolved in water could be quite small. Treatment fluids would essentially tend bypassing these zones of high DNAPL saturation even if the porous medium were inherently quite permeable.

In the subsurface, high permeability pathways commonly facilitate a large flux of treatment chemicals. If these zones contain DNAPLs, the existence of these pathways is an important advantage, maximizing the delivery of treatment chemicals. If the DNAPLs are elsewhere, permeable units can create a hydraulic short circuit, causing the injected oxidants to bypass the zone of interest.

High sweep efficiency is a necessary but not sufficient condition to success in a remedial scheme. Traditionally, the term sweep efficiency defines the fraction of a reservoir that is influenced by the flushing process. However, there is more to treatment than simply having the treatment fluid touch some zone in the medium. A sufficient number of pore volumes have to be delivered to overcome the background consumption and to treat the mass of DNAPLs found there. Ibaraki and Schwartz (2001) developed the concept of "theoretical treatment flux ratio". It is the cumulative magnitude of advective flux of the treatment chemical that reaches points of interest in the zone of contamination as compared to fluxes in the injection wells. Because the treatment flux is defined at various points, contoured cross-sections are useful in illustrating the fluxes of treatment fluids in the system.

Our group has conducted an analysis showing how various types of natural heterogeneity in hydraulic conductivity influence the theoretical treatment flux ratio. Space constraints preclude a complete description of simulation results. However, readers can refer to (Ibaraki and Schwartz, 2001; and Seol et al., 2002) for more information. We illustrate here a few model results.

The simulation problem involves a situation where zone of DNAPL contamination is assumed to be located exactly between the two wells, and is treated via a chemical flood. The hypothetical treatment chemical behaves like a tracer in that it does not react in moving through the system. In effect, the simulations are testing the physical capabilities of the injection system to spread mass through a treatment zone in a complex

porous medium. The injection and withdrawal wells are located 5 meters apart. The pumping is superimposed on a horizontal flow that is moving from left to right. The ambient flow is 30 cm/d.

Here, we illustrate simulation results for a correlated random permeability field with an ln-transformed mean of -23.72 , a variance of 0.9 a horizontal correlation length of 1.8 m and a vertical correlation length of 0.15 m (Figure 1.1a). This particular realization of the field provides for locally high-permeability pathways through the source zone. Two zones short circuit the injection and withdrawal wells. At early time, the flux ratio is > 1 along these zones (Figure 1.1). Elsewhere the flux ratios are low, 0.01 to 0.05 . Thus, most of the clean up is affected within the high permeability zones.

This analysis implies that large volumes of treatment chemicals and many pore volumes will be required to affect DNAPL destruction. The actual quantity of oxidant delivered in a single pore volume is often quite small in comparison with the total mass of DNAPL present in the medium; notwithstanding, the potential for significant losses in reactions with aquifer materials. In effect, a relatively small concentration of oxidant is able to transform only a small quantity of contaminant in a gas or aqueous phase, requiring that the flood be maintained over a relatively long time. Also, the potential exists for considerable volumes of the treatment chemical bypass zones of contamination.

Impact of Chemical Heterogeneities

The term chemical heterogeneity implies geochemical processes that are variable in space and time. The impact of chemical heterogeneity on treatments using chemical oxidants has been the subject of extensive research. At least three chemical processes influence oxidation-based remediation schemes in the subsurface. First, reduced minerals, organic matter, and dissolved organic matter in ground-water reacts with KMnO_4 , peroxide, or Fenton's reagent, as it is transported through the subsurface. These competing reactions require that extra oxidant must be provided to deal with all oxidizable materials, including the contaminants. Chemical heterogeneity also results in variability in the effectiveness of the oxidation process, and in the distribution of reaction products.

Among the different ways in which chemical heterogeneity can impact oxidant delivery, plugging due to the formation of reaction products is one of the most important (Seol et al., 2002). With time, manganese dioxide solid and carbon dioxide gas accumulates in the pores, causing permeability and delivery efficiencies to be reduced.

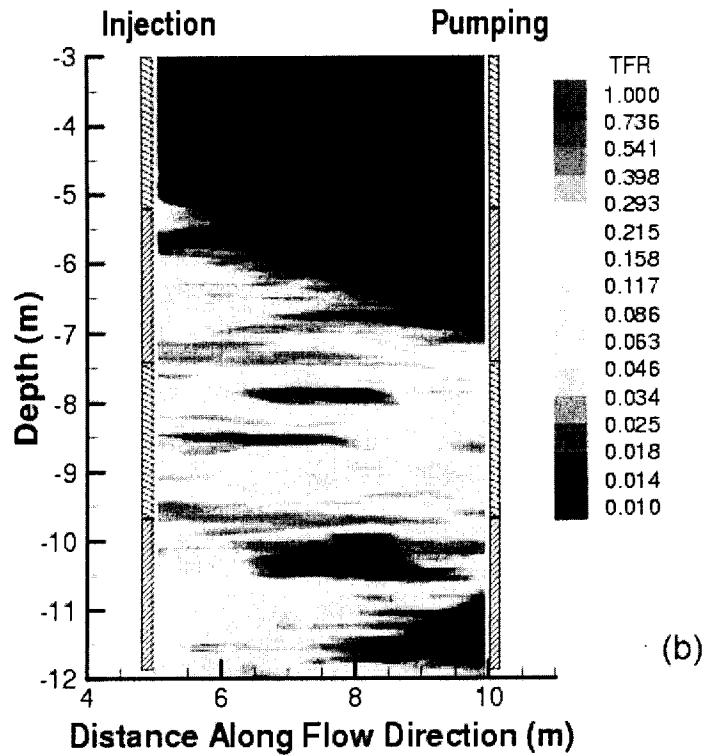
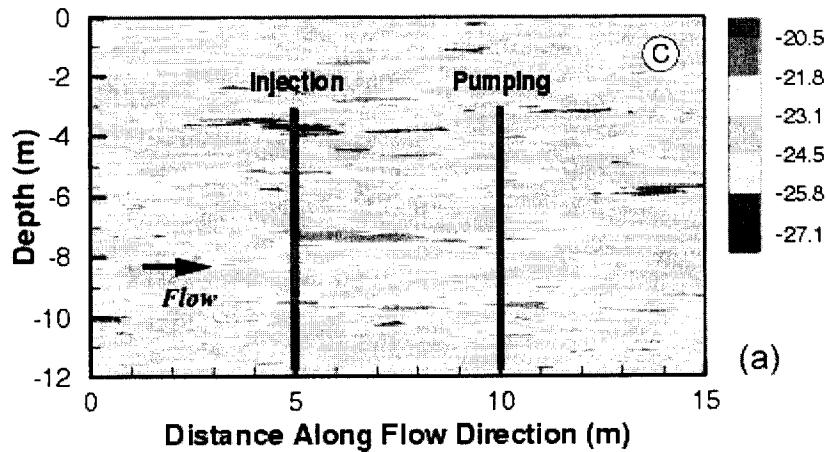


Figure 1.1 Flooding of the heterogeneous medium (Panel a) with at least two permeable pathways would yield the distribution in the treatment flux ratio (TFR) shown in Panel b (modified from Ibaraki and Schwartz, 2001).

Plugging will be most serious within the zone of contamination, where DNAPL saturations can be relatively large. Figure 1.2 is a photograph from an experiment conducted Conrad et al. (2002), showing this problem of chemical heterogeneity. In a

two-dimensional flow tank constructed with a heterogeneous medium, they created zones of locally high TCE saturation (red areas, Figure 1.2). After minimal flooding with 1 gm/L, KMnO_4 , low permeability rinds of MnO_2 (brown color in Figure 1.2) formed and sequestered the TCE from further contact with the oxidant. There is no remedial advantage to this encapsulation. Conrad et al. (2002) found that once MnO_4^- flooding was halted, TCE slowly leaked out of these zones. Li and Schwartz (2000) obtained similar results using a small 2-D glass flow tank packed with clear 1mm borosilicate glass beads.



- Sand
- Red-stained TCE in lense
- MnO_2 rind

Figure 1.2 This photograph shows rinds of MnO_2 (brown) that form around zones having high saturations of TCE (red) after flooding with KMnO_4 . The low permeability rinds isolate the TCE from the oxidant. The tank is 60 cm long (from Conrad et al., 2002).

Conclusions

In spite of the promise of various approaches to in situ chemical oxidation, there are problems of efficiency that will likely plague most deployments. These problems are now being observed in laboratory demonstrations and computer-based experiments, where it is possible to observe processes in detail. In general, most field demonstrations or site cleanups are not adequately instrumented to discover these problems.

Physical and chemical heterogeneities in the subsurface work against bringing the oxidant to zones of high concentrations. The highly heterogeneous distribution of contaminants and difficulties in characterization make it difficult to target specific zones for treatment. Thus, often, large volumes of sediments will be treated whether

contaminated or not. Heterogeneities in hydraulic conductivity at most sites provide intensive flooding of permeable pathways and little treatment of low conductivity zones. Reaction products (e.g., CO₂ gas, MnO₂) tend to plug the porous medium, especially in zones with large saturations of pure-phase contaminants. With time, the oxidant flood is diverted away from these zones of large contaminant saturations.

2. Increasing DNAPL Removal Rate Through Treatment of Mn Oxide Precipitates

Previous studies on in situ chemical oxidation of trichloroethylene (TCE) with potassium permanganate (KMnO₄) indicated that the solid reaction product, Mn oxide could reduce the permeability of the porous medium and impact the success of DNAPL removal. In order to address the issue of permeability reduction caused by precipitation, we investigated the mineralogy of Mn oxides, and the possibilities of controlling the colloid growth and removing the solid precipitates by dissolution. We also conducted flow tank experiment to test scheme that increases DNAPL removal efficiency by dissolving Mn oxide precipitates.

Mn oxide mineral identification and property measurement

Mn oxide was prepared by mixing TCE with KMnO₄ solution in laboratory condition. A SEIKO SSC 5020 instrument (Haake Inst., Paramus, NJ) with a TG/DTA simultaneous analysis module, model 200 was used for thermal gravimetric (TG) and differentiated thermal analysis (DTA). The weight loss in the sample at temperatures above 125 °C is considered to be due to the loss of structural water. Dissolved Mn oxide was analyzed with ICP-MS (Inductively Coupled Plasma Mass Spectrometer) to determine the concentration of manganese and potassium within the Mn oxide. The chemical formula of the Mn oxide is determined as K_{0.854}Mn_{1.786}O₄•1.55H₂O based on thermal analysis and ICP-MS. The chemical composition obtained from this study seems reasonable, and is comparable with other results.

X-ray diffraction powder analysis was performed with a Philips diffractometer (Philips Elec. Inst., Mahwah, NJ) using CuK α -radiation and vertical, wide-range goniometer equipped with a diffracted beam monochromator and a theta-compensating slit. The X-ray diffraction (XRD) spectrum (Figure 2.1) for the synthetic Mn oxide shows no prominent peak, indicating that the solid is not well crystallized. However, the pattern matched birnessite in the database in general, and had a clear but not very intense peak at 7.3 Å. The 7 Å interlayer spacing is the typical birnessite spacing, and identify it as the characteristic feature for birnessite. Because the mineral is formed in a potassium rich environment, the mineral formed in the oxidation of TCE by MnO₄⁻ is semi-amorphous potassium-rich birnessite.

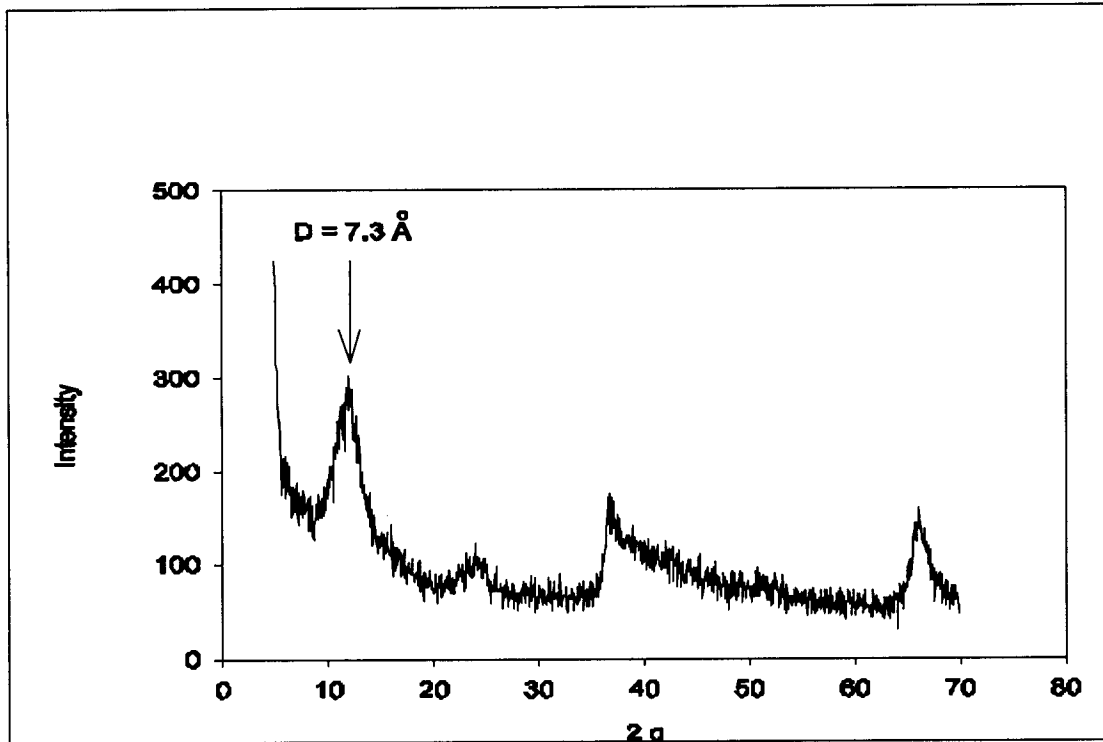


Figure 2.1 Spectrum of X-ray diffraction analysis of the Mn oxide. Peak at 7.3 Å indicates the interlayer spacing of the mineral.

A Philips CM-200 TEM (transmission electron microscope) was used to directly examine the fine structure of the mineral. TEM analysis found that the Mn oxide crystal is a cluster of small needles (Figure 2.2). These findings confirm earlier XRD results that the crystal structure of Mn oxide is poorly developed. TEM chemical composition analysis also identified K and Mn as the only major metal cations in the mineral.

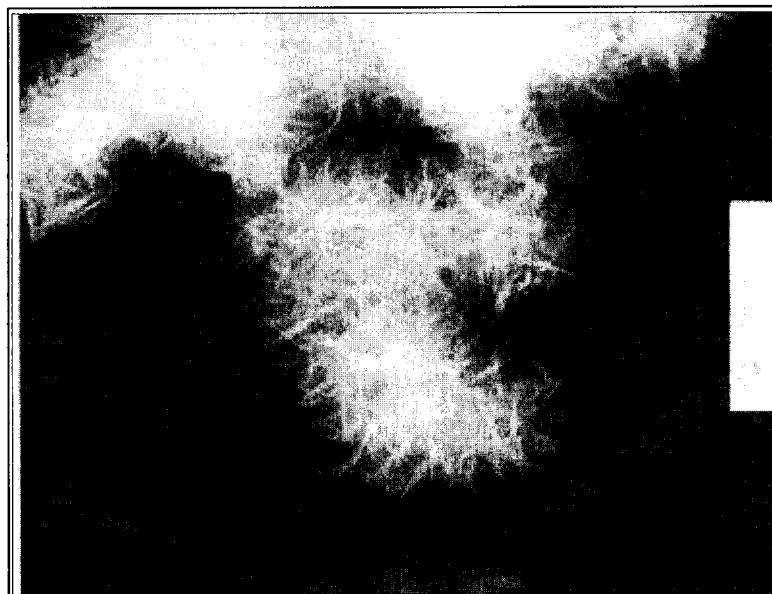


Figure 2.2 Results of the TEM analysis for the Mn oxide powder. The white fibrous material in the picture is a cluster of small needle-shaped crystals of the mineral.

The basic structural unit for birnessite is a sheet of MnO_6 octahedral (Figure 2.3). The interlayer cations and water molecules generally occupy different positions in each of the three phases. The H_2O molecules in the mineral mostly occur in the interlayer. However, some of them can be present as OH^- . Sometimes, this birnessite is called manganese (hydro)oxide.

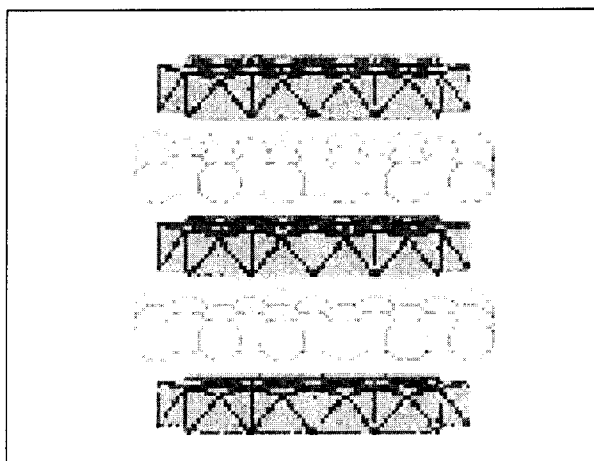


Figure 2.3 Polyhedral representations of crystal structures of Mn oxide minerals formed during ISCO with MnO_4^- . K-rich birnessite-like phase showing disordered $\text{H}_2\text{O}/\text{K}$ (light color ball) sandwiched between the Mn octahedral sheets.

The surface chemical properties were measured for the Mn oxide. Specific surface area of the Mn oxide powder was determined using a liquid nitrogen adsorption (BET)

method. The Mn oxide has a relatively small specific surface area at $23.6 \pm 0.82 \text{ m}^2/\text{g}$. The point of zero charge (pzc) of the Mn oxide was measured as 3.7 ± 0.4 using potentiometric titration method. This birnessite is a relatively active species and could participate in various reactions with existing organic and inorganic matter.

Phosphate as an inhibitor of the formation of colloidal Mn oxide

Since Mn oxide forms colloid before precipitates out as solid from the aqueous phase, one possible approach to address the problem of pore plugging is to control the rate of colloid formation. Phosphate ions have large charges, and are reported to tend to sorb on colloid. It may be applied to the oxidation reaction to influence the surface charge of colloidal Mn oxide, thus the coagulation process. In this study, we utilized batch experiments to explore the feasibility of applying phosphate to slow down the formation of colloidal Mn oxide. UV-vis spectrophotometer and photon correlation spectroscopy were used to monitor the process of colloid formation as oxidation is occurring. The surface charge of the colloid was quantified with zeta potential measurements. The results show that phosphate can slow down the formation of the colloids, especially early in the reaction. The rate of the colloid formation decreases linearly with increasing concentrations of phosphate ion for the range of concentrations in our experiments (Figure 2.4).

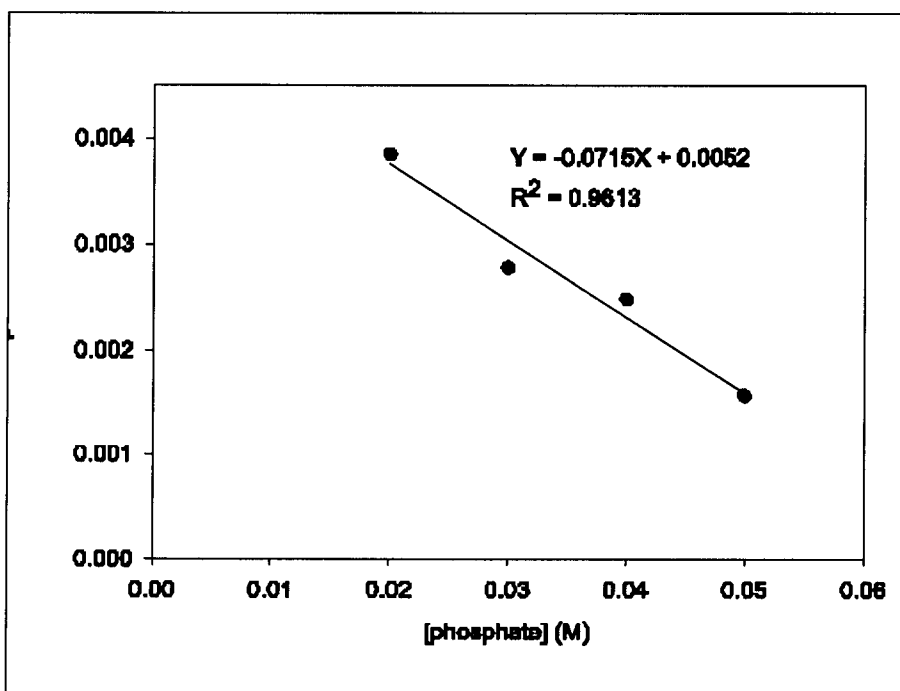
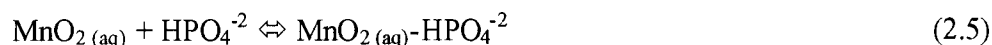
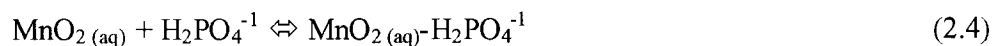
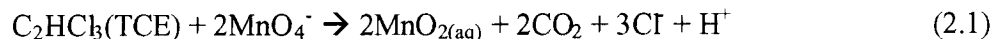


Figure 2.4 Colloid growth rate ($1/T_p$) versus phosphate concentration ($[\text{K}_2\text{HPO}_4]=[\text{KH}_2\text{PO}_4]$).

Efforts were made to elucidate the reaction mechanism of the interaction between phosphate and Mn oxide. The process is thought to involve the formation of a Mn(IV)-

phosphate complex in the aqueous phase before formation of the colloids. A model was proposed to describe the reaction process which involves following reactions :



where $\text{MnO}_{2(\text{aq})}$ is dissolved Mn(IV) species; $\text{MnO}_{2(\text{c})}$ is colloidal Mn oxide; $\text{MnO}_{2(\text{s})}$ is the Mn oxide precipitates. $\text{MnO}_{2(\text{aq})}\text{-H}_2\text{PO}_4^{-1}$ and $\text{MnO}_{2(\text{aq})}\text{-HPO}_4^{-2}$ are Mn(IV)-phosphate complexes. As oxidation of TCE begins, dissolved Mn oxide ($\text{MnO}_{2(\text{aq})}$) is first produced. Then $\text{MnO}_{2(\text{aq})}\text{-H}_2\text{PO}_4^{-1}$ and $\text{MnO}_{2(\text{aq})}\text{-HPO}_4^{-2}$ are formed. When phosphate in solution was used up or Mn(IV)-phosphate complexes dissociate, colloids coagulate and precipitate.

The results also indicate that the colloid coagulation rate increases with the increasing ionic strength. Our study provides scientific background on the possibility to slow down the formation of colloid during the oxidation scheme by chemical additives. With more understanding on this treatment, it is possible to apply the principle of this study to mitigate the problem of pore plugging and permeability reduction in the ISCO scheme.

Dissolution of Mn oxide in organic acids

Certain organic acids can enhance the dissolution of Mn oxide precipitates. The dissolution kinetics of Mn oxide was evaluated in batch experiments using solutions of citric acid, oxalic acid, and EDTA. Initial dissolution rates were determined to be 0.126 mM/m²/h for citric acid, 1.35 mM/m²/h for oxalic acid, and 5.176 mM/m²/h for EDTA. These rates compare with 0.0025 mM/m²/h for nitric acid at pH = 2 (Table 2.1). Organic acids dissolve Mn oxide quickly. Reaction rates increase with acid concentration, as tested with citric acid (Table 2.2).

Table 2.1 Initial rate of dissolution of Mn oxide with various acids at pH = 2.

Acids	Citric	EDTA	Oxalic	Nitric
R (mM/m ² /h)	0.126	5.176	1.350	0.0025

Table 2.2 Initial rate of dissolution of Mn oxide with citric acid at various concentrations, pH = 2.

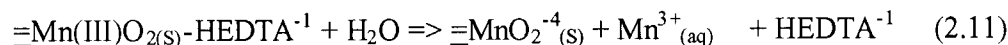
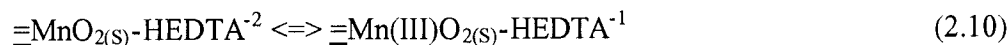
Concentration	0	0.05 mM	0.1 mM	0.2 mM
R (mM/m ² /h)	0.0025	0.0209	0.126	0.254

The Mn oxide dissolution mechanism likely involves proton and ligand-promoted dissolution and reductive dissolution. Citric and oxalic acid can induce ligand-promoted dissolution. With a model we propose, the dissolution reaction with the citrate and oxalate can be conceptually described by Equations 2.6, 2.7, and 2.8.



where L represents the ligands, which can be citrate or oxalate. The first reaction (Equation 2.6) involves the binding of the ligand to the surface. The second (Equation 2.7) involves the dissolution of Mn from the solid. With the third reaction (Equation 2.8), the surface is restored.

EDTA can induce ligand-promoted and reductive dissolution. We propose the following model for the dissolution of Mn oxide by EDTA (Equations 2.9 to 2.12).



where HEDTA^{-1} and HEDTA^{-2} are general representations of EDTA species in the solution at low pH. Equation 10 is the electron transfer step for the reduction of Mn(IV) to Mn(III). Step three is the detachment process and is expected to be slow and rate limiting. The Mn^{3+} species is short-lived and further reduced to Mn(II) in the solution (Equation 2.12).

At low pH, proton-promoted dissolution seems to occur with all the acids tested, but this process is not dominant. Reductive dissolution appears to be the most effective process in dissolving the solid, followed by ligand-promoted dissolution. These experiments indicate the significant potential in using these organic acids to remove precipitates formed during the oxidation reaction.

Increasing DNAPL removal efficiency by dissolving Mn oxide precipitates

With the understanding of fundamental dissolution mechanism, we conducted 2-D flow-tank experiments to examine the possibility of nearly complete DNAPL removal by ISCO with MnO_4^- , when organic acids are used to remove Mn oxide. The experiments were conducted in a small 2-D glass flow tank containing a lenticular silica-sand medium. Blue dyed trichloroethylene (TCE) provided residual, the perched and pooled DNAPL. KMnO_4 at 200 mg/L was flushed through the DNAPL horizontally. Once plugging reduced permeability and prevented further delivery of the oxidant, citric or oxalic acids were pumped into the flow tank to dissolve the Mn oxide precipitates. Organic ligands removed the Mn oxide precipitates relatively quickly, and permitted another cycle of MnO_4^- flooding. Cycles of MnO_4^- /acid flooding continued until all of the visible DNAPL was removed. The experiments were monitored with chemical analysis and visualization. A mass-balance calculation indicated that by the end of the experiments, all the DNAPL was removed. The results show also how heterogeneity adds complexity to initial redistribution of DNAPL, and to the efficiency of the chemical flooding.

The flow tank experiment confirmed the possibilities of restoring permeability damaged by Mn oxide precipitation. This restoration process proceeded relatively quickly, even in the face of complexities related to the heterogeneous medium, the broad initial distribution of the DNAPL and the chemical heterogeneities provided by the pore plugging. With the first cycle of MnO_4^- flooding, there was only minimal destruction of TCE, about 5%, before plugging brought flushing to a halt. This experience reinforces results from other experimental studies suggesting that plugging would be serious problem with *in situ* MnO_4^- oxidation schemes. However, in a large, three-dimensional system, the loss of flooding efficiency may not be so apparent as with a simpler and more constrained tank experiment. Also, the extent of plugging depends on the original DNAPL distribution. Clearly, ISCO with MnO_4^- performs better in removing residual than pooled DNAPL.

There seem to be good possibilities for using citrate and oxalate to control plugging created by the precipitation of Mn oxide. The practical dissolution rate however would be much less than measured in batch experiments. The combination of ISCO and the dissolution of DNAPL during the acid flush led to nearly complete destruction of DNAPL. Clearly, this technique needs to be tested in more realistic conditions. There are scale effects in dissolution to be explored, along with interactions between the organic acids and the porous media.

3. Destruction Efficiencies and Dynamics of Reaction Fronts

In spite of promising results in field applications of KMnO_4 flushing scheme, some researchers have identified plugging problems from the reaction products, i.e., MnO_2 precipitates and CO_2 gas (Schnarr, M., et al, 1998; Schroth, M.H., et al., 2001; Reis, J.C. and Acock, A.M., 1994; Li, X.D. and Schwartz, F.W, 2000). For example, Schroth et al. (2001) reported from column experiments that the formation of MnO_2 and CO_2 gas decreased the relative permeability of the porous medium by ~53 to ~90%. In 2-D flow tank experiments, Li and Schwartz (2000) found that the DNAPL mass removal

rate by permanganate flushing was greatest in the early stages of flushing, but decreased dramatically as the treatment proceeded. They attributed this result to increasing flow divergence around zones of higher DNAPL saturation as MnO_2 precipitates and CO_2 gas reduced permeability in these zones. This localized plugging over time is sufficient to prevent the efficient delivery of MnO_4^- solution to zones of high TCE saturation.

To delineate plugging problems and estimate the efficiency of KMnO_4 flushing scheme for destroying chlorinated solvents in groundwater, we performed a large scale ($L \times W \times D = 180 \text{ cm} \times 60 \text{ cm} \times 90 \text{ cm}$) 3-D flow tank experiment (Figure 3.1). Specifically, we focused on monitoring the formation and distribution of MnO_2 precipitates using optical and chemical monitoring techniques to describe clean-up progress and the space/time dynamics of the solid-phase oxidation reaction front. Details of the experimental setup and procedures are described in Lee et al. (2003), which is attached to this report as a journal publication.

In situ monitoring of color patterns in the porous medium provided a basis for characterizing the progress of reactions. Figure 3.2 illustrates the typical pattern of zonation with a vertical cross section through the TCE source zone. The purple colored zones on top and bottom indicates the presence of essentially unreacted KMnO_4 solution in the pores. Black coloration formed in the boundary zones between the colorless zones of TCE source and unreacted KMnO_4 solution indicating a zone of MnO_2 deposition. Similar zonation was evident throughout the tank, as determined using images collected from the glass wells. Evidently, a zone of MnO_2 surrounds the dissolved TCE plume on the top and bottom and both sides. Photos of the excavated surfaces provide horizontal views of the porous medium at different depths (Figure 3.3). Clearly, MnO_2 precipitates are evident in the TCE source zone. They are also associated with the dissolved TCE plume downstream of the source. Note how in several of the horizontal slices, the MnO_2 was concentrated along a region corresponding with the likely edge of the TCE plume, downstream from the source. The zone coinciding with the interior of the plume has a lighter purple color.



Figure 3.1 3-D plastic tank used for the KMnO_4 flushing experiment

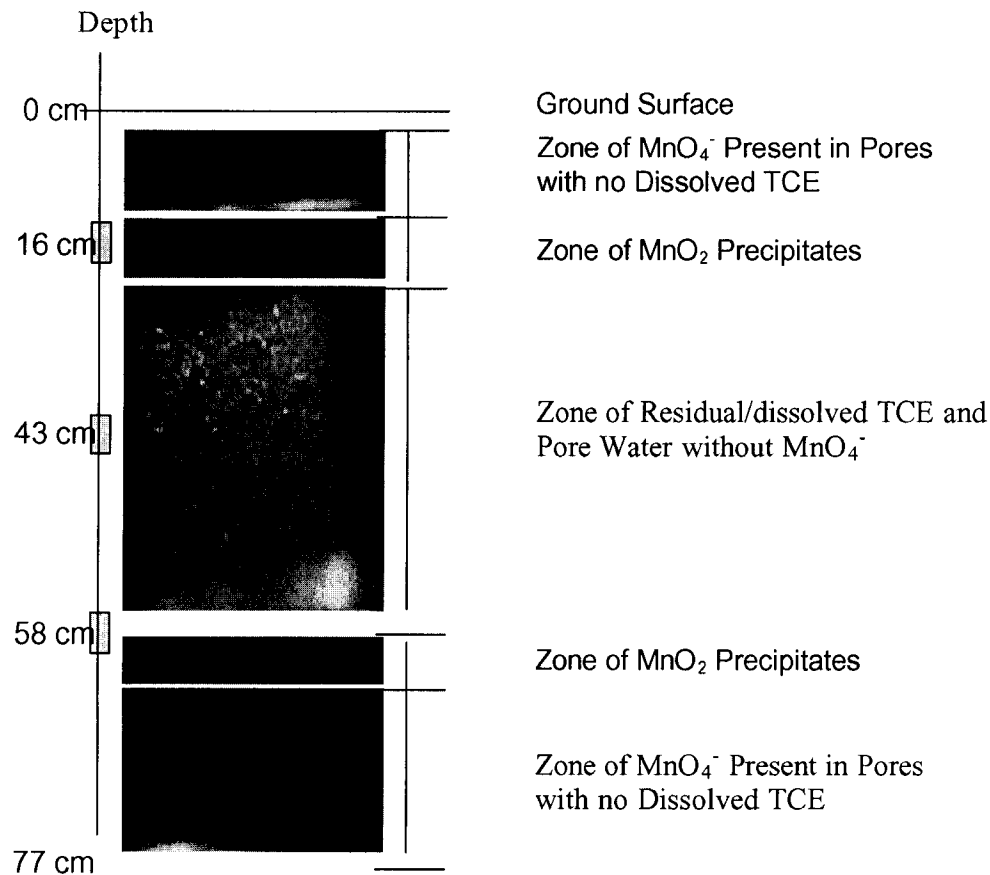


Figure 3.2 Vertical cross section showing the reaction front formation in the TCE source

Spatial and temporal development of MnO_2 reaction front over time (Figure 3.4) shows a decrease in the reaction-front velocity over time within the source and down gradient. This was attributed to MnO_2 plugging of porous media around the TCE source and plume. The decrease in the reaction-front velocity over time indicated that the DNAPL oxidation process became more and more inefficient with time. The TCE plume diminished in size considerably over time (Figure 3.5). This observation was in keeping with the zonal change patterns of the down-hole optical data over time and distance and the reaction-front dynamics, indicating general inefficiency in the delivery of MnO_4^- through the MnO_2 zone to the TCE plume. Distributions of MnO_2 precipitates in the flow tank indicated that TCE destruction was more active in and immediately adjacent to the source than further downstream. This observation was in keeping with the data from the down-hole optical measurements and the TCE concentration contours. We performed mass-balance calculations using the MnO_2 concentrations data collected throughout the flow tank after flushing was completed. Based on our mass-balance calculation, the total

mass of TCE oxidized in flushing with 3213 liters of permanganate solution (1250 mg/L) was estimated to be approximately 297 g, which was about 41% of the total TCE emplaced in the source zone. This calculation indicated that only 18% (~570 L) of permanganate solution (1250 mg/L) applied to the DNAPL zone was used for the oxidation reaction.

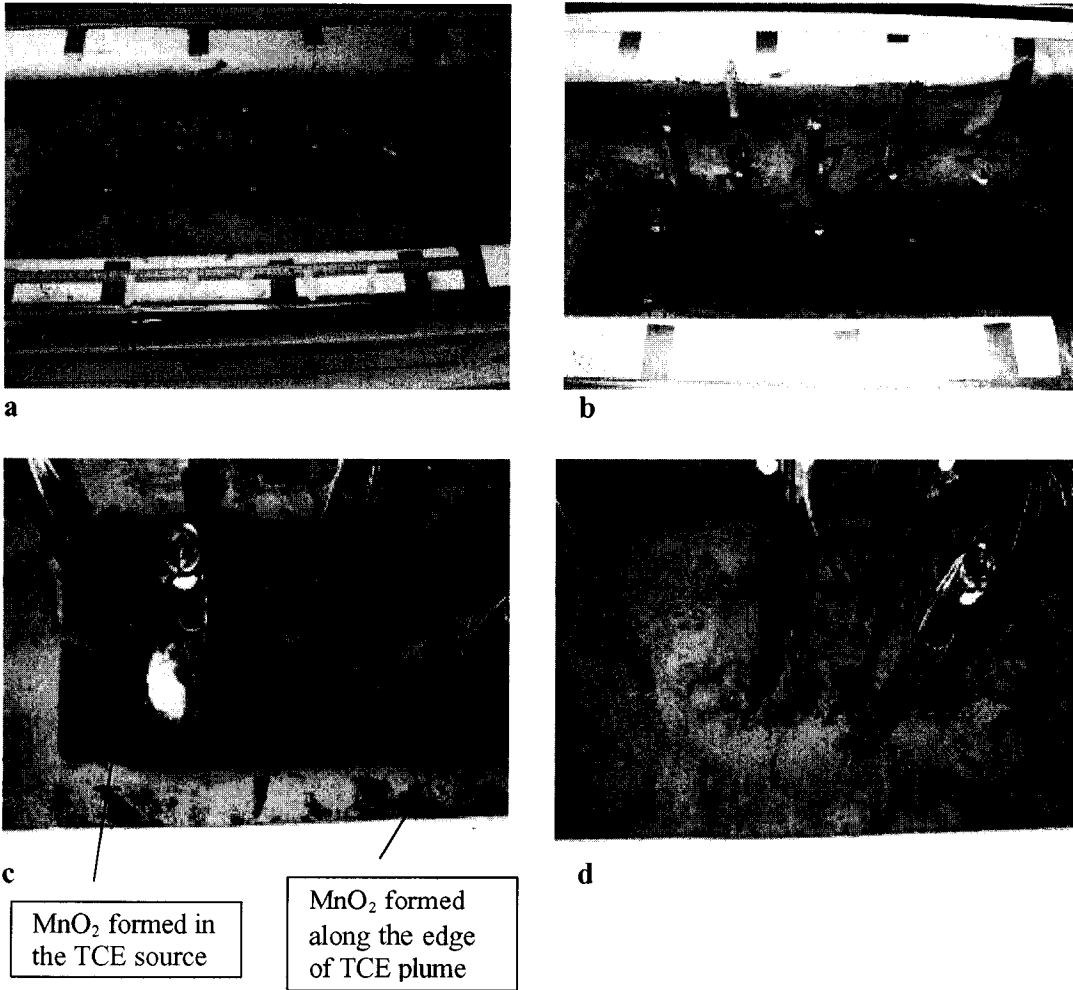


Figure 3.3 Photos showing the excavated surface of the sands

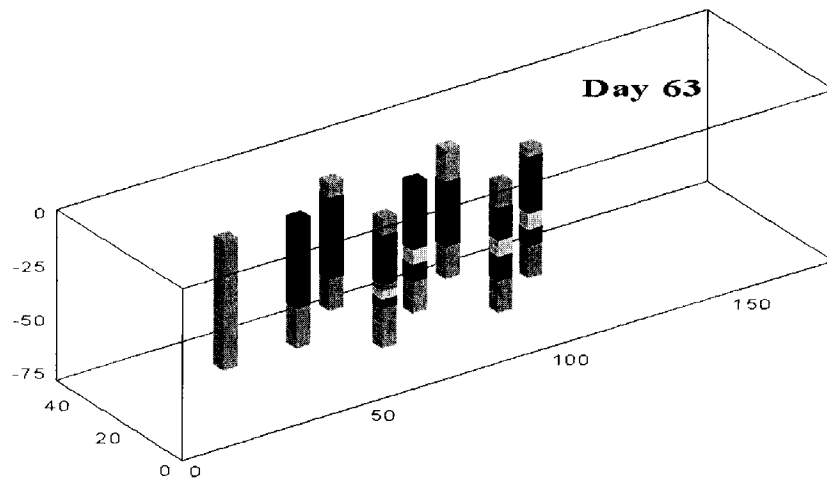
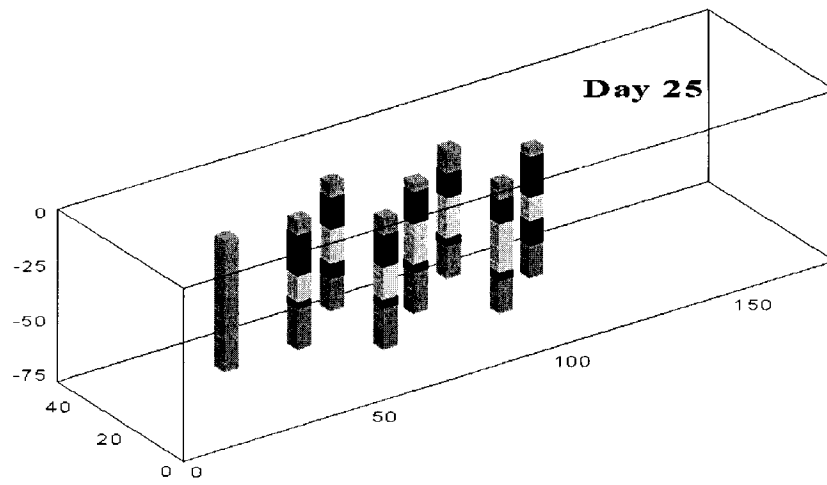


Figure 3.4 Reaction-front dynamics in the flow tank

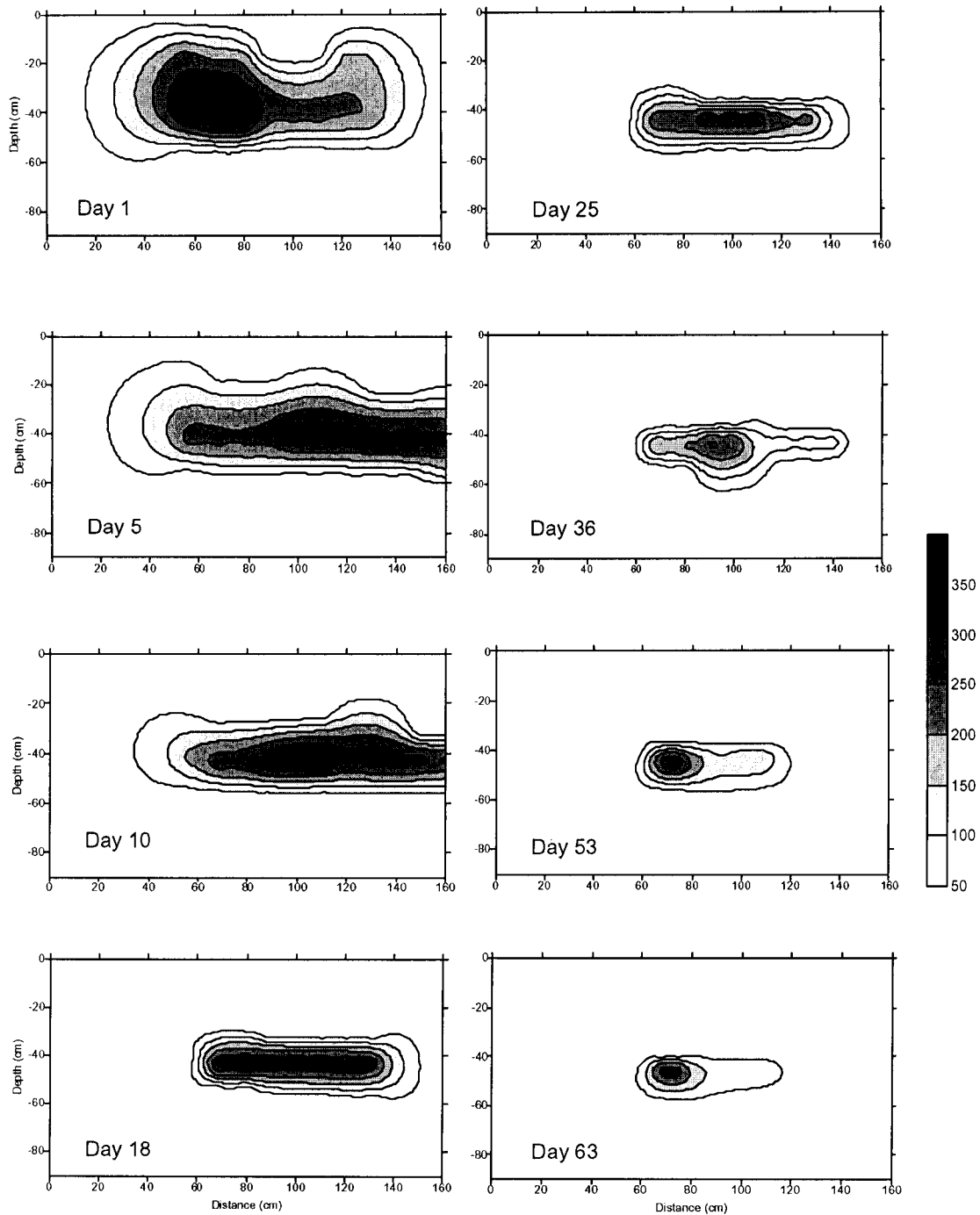


Figure 3.5 Temporal and spatial variations in the TCE contours

Our results showed that the efficiency of the KMnO_4 treatment of chlorinated solvents in the flushing scheme diminished with time due to the formation of low-permeability reaction zones in the TCE source and along the downstream edge of the TCE plume. In addition, large amount of unreacted KMnO_4 solution left the

contaminated zone during the flushing activity. This excess KMnO_4 may provide a source for secondary contamination to the aquifer. These results support our suggestion that a development of a new KMnO_4 treatment scheme that could provide both contaminant destruction and plugging/permanganate control is required.

4. Computer Model Development

An integral part of the study involved continued development of the ISCO3D computer code, which began with our previous of the previous EMSL grant. At the end of that study, a preliminary version of the code was operational (Zhang and Schwartz, 2000), but relatively rudimentary. Major emphases in the initial part of the present study were to improve the input/output structure of the code to make it more user friendly, to document the verification and other test problems, and to develop a detailed user's guide for the code. Completion of this aspect of the study led to the production of a 96 page Users Guide, which we will discuss here in more detail.

One of the significant limitations with the code was an inherent assumption that porosity and permeability were assumed not to change as products (solids, gases) from the destruction of the particular chlorinated solvent accumulated in the pores. This assumption is probably valid for problems in coarse porous media where DNAPL saturations are low. However, our experiments provided examples of situations where extensive plugging of the porous medium is evident. Thus, another emphasis in the present study was to modify the code to account for changes in permeability and porosity due to the reactants. This section will describe these modifications to the code and some of the test cases that were run.

Description of the Computer Model:

General Formulation

The ISCO3D code was developed originally to simulate the coupled processes of NAPL dissolution, chemical reactions, and solute mass transport in the in-situ chemical oxidization scheme (Zhang and Schwartz, 2000). The model incorporates a kinetic description of reactions between the MnO_4^- and the chlorinated ethylenes and the rate of dissolution of the NAPL. It is also capable of simulating the key reactions between aquifer material and permanganate and the kinetic sorption of chemicals, and has been optimized for computational efficiency. A detailed description is provided in previous papers and reports. Here, we provide readers with a brief overview.

The code is specifically developed to describe a problem of contamination with residual NAPL or a dissolved plume of chlorinated compounds in the saturated zone. MnO_4^- is injected into the aquifer with wells and assumed to spread. The code incorporates MnO_4^- reactions with solid organic carbon and other relatively oxidized solids in the porous medium, as well as the dissolved chlorinated compounds in the aqueous phase.

The modeling approach involves solution of coupled flow and transport equations. Assuming that the NAPL is immobile and the saturation of the NAPL in the medium is small, the ground-water flow equation can be written as (Bear, 1972; Frind, 1983)

$$\nabla(\mathbf{K} \nabla h) + Q = S_s \frac{\partial h}{\partial t} \quad (4.1)$$

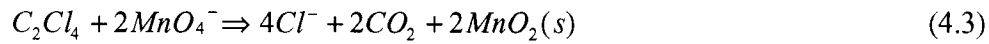
where \mathbf{K} is the hydraulic conductivity tensor (L/T), h is the water head (L), Q is the source (L^3/T), t is time (T), and S_s is specific storage (L^{-1}).

The mass-transport equation (modified from Bear, 1972; Huyakorn and Pinder, 1983) for mobile species is expressed as

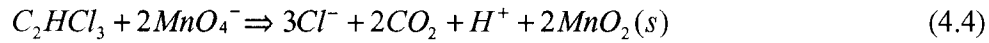
$$\nabla(n\mathbf{D}\nabla c_i) - \nabla(nV c_i) + r_i = \frac{\partial(n c_i)}{\partial t} \quad (4.2)$$

where n is porosity, \mathbf{D} is the dispersion coefficient tensor (L^2T^{-1}), V is the linear groundwater velocity vector (LT^{-1}), c_i is the concentration for species i (ML^{-3}), and r_i is the reaction rate for species i ($ML^{-3} T^{-1}$). The code includes the chemical reactions between MnO_4^- , one of the NAPLs, like tetrachloroethene (PCE), trichloroethene (TCE), or dichloroethene (DCE), and aquifer material (for example, solid organic carbon). These chemical reactions are written as follows:

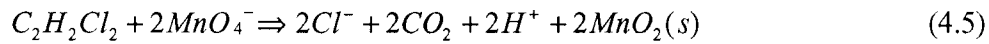
(a) PCE



(b) TCE



(c) DCE



(d) Solid organic carbon



(e) Sorption reaction



The reactions with the chlorinated compounds are assumed to be kinetic, while those involving solid organic matter and sorption are kinetic. A detailed description of the formulation of these equations is presented by Zhang and Schwartz (2000)

Kinetic Dissolution Model for NAPLs

When pure phase NAPL is present in the subsurface, it dissolves slowly and might act as a source for hundreds of years. In the code, a sub-model that incorporates key controlling parameters simulates this slow release. The rate of organic dissolution can be described by

$$n \frac{dc_i}{dt} = k_{Ni} (c_{Si} - c_i) \quad (4.8)$$

where c_i is the aqueous concentration corresponding to NAPL species i (ML^{-3}), k_{Ni} is the mass transfer coefficient (T^{-1}), and c_{Si} is the equilibrium concentration with pure organic liquid or solubility of species i (Pfannkuch, 1984; Sleep and Sykes, 1989; and Miller et al., 1990). Zhang and Schwartz (2000b) provide details of this correlation approach

Solution Procedures and Mathematical Formulation

In this study, a sequential non-iterative approach was used to solve the transport and reaction equations in separate steps. To improve the accuracy, a time-centered method, Strang splitting, was used to couple the physical transport and chemical reactions. Strang splitting is similar to the alternating operator-splitting scheme proposed by Valocchi and Malmstead (1992) to reduce mass balance errors. In the Strang-splitting approach, changes in solute mass are calculated in two transport time steps and one reaction time step. Overall, there are seven different steps in the solution procedure (Zhang and Schwartz, 2000b). The flow and transport equations were discretized by the finite-volume method.

The approach also requires solution of a coupled system of kinetic reactions. We adopted a predictor-corrector procedure developed by Zysset et al. (1994). Zhang and Schwartz (2000b) discussed the many issues that need to be addressed in making this approach feasible in terms of execution times for multi-dimensional problems.

Model Verification and Demonstration

Our previous final report and various papers (e.g., Zhang and Schwartz, 2000a and 2000b) discussed various aspects of code verification and demonstration in detail. Accordingly, we will briefly summarize the types of numerical experiments without a detailed analysis. The first verification experiment sought to reproduce column flushing experiments by Schnarr et al. (1998), using aquifer materials from the Canadian Forces Base Borden. Figure 1 shows the simulation domain and basic data for the five column experiments. This 1-D simulation was discretized by 40 rectangular blocks with $\Delta x = 0.01$ m, and $\Delta y = \Delta z = 0.045$ m. The basic characteristics of the breakthrough curves of CI were simulated reasonably well, although there were some differences between the measured and the calculated breakthrough curves.

The second, three-dimensional simulation sought to match the CI mass production rate in a field test designed as a proof-of-concept of source-zone flooding by MnO_4^- (Schnarr et al., 1998). The demonstration is based on a field-scale experiment at CFB Borden that demonstrated the potential of MnO_4^- flooding for removing pure-phase PCE (Schnarr et al., 1998). The simulated mass removal rate in terms of CI was compared with measurements. The two results exhibited a relatively close match after trial and error adjustment of reaction parameters. Interestingly, the mass removal rate could not be simulated without accounting for MnO_4^- oxidation of the aquifer materials. Thus, it is clear that a major factor affecting the transport of the MnO_4^- front is the quantity of reactive materials present in an aquifer.

The third set of simulations was based on a similar field-demonstration of KMnO_4 flooding at a DOE facility (West et al., 1997). A field-scale experiment of MnO_4^- oxidation of TCE was performed at the Department of Energy Portsmouth Gaseous Diffusion Plant (PORTS) in Ohio by researchers from Oak Ridge National Laboratory (ORNL) (West et al., 1997). Readers can refer to West et al. (1997) for details of the physical setting and actual test. A two-dimensional model of 51x51 nodes was constructed to represent the treatment zone and its vicinity. The simulation grid was

designed with relatively small node spacings inside the test region ($\Delta x = 1$ m, and $\Delta y = 2$ m) and relatively large spacings outside (max. $\Delta x = 6$ m, and max. $\Delta y = 7.5$ m).

The simulation indicates that dissolved TCE concentrations were significantly reduced, where the MnO_4^- was delivered, as compared to the initial TCE concentration. Generally, the simulated results matched well with experimental measurements. The computer model provides a useful tool for assisting the design and the prediction of the oxidization processes under field conditions.

User's Guide for Code

We have developed a User Guide for USCO3D to support its utilization by other organizations. The guide is divided into three chapters. Chapter 1 is an overview that describes the general formulation of the code, the treatment of kinetic reactions, a description of the finite volume formulation, and the special approaches for treating kinetic reactions. Chapter 2 is a detailed description of the procedures for entering parameter values, and a description of the output files. This chapter also describes the use of utility programs for extracting particular information from the model output for plotting.

The final chapter describes three worked examples along with the data sets required to run these problems. The three examples are the one, two and three-dimensional cases discussed previously, which are all based on actual field examples.

Coupling Flow and Mass Transport Processes

This section describes the approach used to provide coupling between flow and transport due to the formation of reaction products, particularly MnO_2 . These modifications build on the theory and numerical procedures for reactive transport presented by Zhang and Schwartz (2000b). Coupling due to precipitation of MnO_2 is accounted primarily in the reduction in the porosity and permeability of the medium.

The calculation of porosity by the precipitation of MnO_2

$$n_{new} = n_{old} \times \left(1 - \frac{C_{MnO_2}}{\rho_{MnO_2}}\right) \quad (4.9)$$

where ρ_{new} and ρ_{old} are the porosities of the media before and after the precipitation of MnO_2 , respectively. The C_{MnO_2} is the quantity of MnO_2 precipitated in pores per volume of pores. The ρ_{MnO_2} is the density of MnO_2 .

The calculation of porosity also needs to account for the presence of any NAPL in the pore. Mathematically, this correction is expressed as

$$n_{new} = n_{old} \times (1 - S_{TCE}) \quad (4.10)$$

where S_{TCE} is the saturation of TCE NAPLs. The calculation of permeability by the precipitation of MnO_2 is given as

$$k_{new} = k_{old} \times \left(\frac{n_{new}}{n_{old}}\right)^3 \left(\frac{1-n_{old}}{1-n_{new}}\right)^2 e^{-n_{factor} \left(\frac{n_{old}-n_{new}}{n_{old}}\right)} \quad (4.11)$$

where k_{new} and k_{old} are the permeabilities of the media before and after the precipitation of MnO_2 , respectively. The n_{factor} is the coefficient factor or

$$k_{new} = k_{old} \times \left(\frac{n_{new}}{n_{old}}\right)^3 \left(\frac{1-n_{old}}{1-n_{new}}\right)^2 e^{-n_{factor} \left(\frac{n_{old}-n_{new}}{n_{old}}\right)} \quad (4.12)$$

The calculation of permeability in the presence of NAPL is expressed as

$$k_w = k_s \times \left(\frac{1-S_{NAPL}-S_{wr}}{1-S_{wr}}\right)^4 \quad (4.13)$$

When the saturation of NAPL is 0, the permeability of the media will be that of single fluid (water).

One-Dimensional column experiments

As part of a series of laboratory experiments, we conducted a series of small-scale column experiments. In these experiments, a fixed quantity of TCE was placed at the bottom of a short column. The column was flooded in an upward direction with a solution of MnO_4^- . In these experiments, parameters that were adjusted. Table 4.1 and 4.2 summarize the setup and conditions of the column experiments.

Table 4.1. Setups for column experiments

Experiment	Dimension (mm)	Medium	Q (mL/min)	Porosity
Column A	85(L)x8(ID)	Silica sand	Vary	0.385

Table 4.2. Conditions for column experiments

Column	DNAPL (g TCE)	Q (ml/min)	C (KMnO ₄) (g/L)	Total KMnO ₄ load (g)
A-1	0.2924	0.038	0.1	0.027
A-2	0.2924	0.057	0.1	0.040
A-3	0.2924	0.094	0.1	0.066
A-4	0.2924	0.129	0.1	0.091
A-5	0.2924	0.235	0.1	0.17

Simulation of Column Experiments

The following series of model trials are designed to demonstrate the ability of the code to simulate flow and transport as the porous medium in the column gradually becomes plugged due to the breakdown of TCE.

Shown in Figure 4.1 is a schematic representation of the simulation domain. The one-dimensional grid consists of 40 blocks in direction of flow. The grid blocks have the following dimensions, $dx = 0.002125$ m, $dy = dz = 0.00709$ m. At the right end of the domain, the boundary condition for flow is a constant head at nodes 81, 82, 163 and 164. Applying a constant flux at nodes 1, 2, 83, and 84 the boundary condition at the left end. All the other sides are no-flow boundaries. The porous medium is assumed to have a porosity of 0.385 and a permeability of 8×10^{-8} m². The dispersivity values are $\alpha_L = \alpha_T = \alpha_V = 0.002$ m.

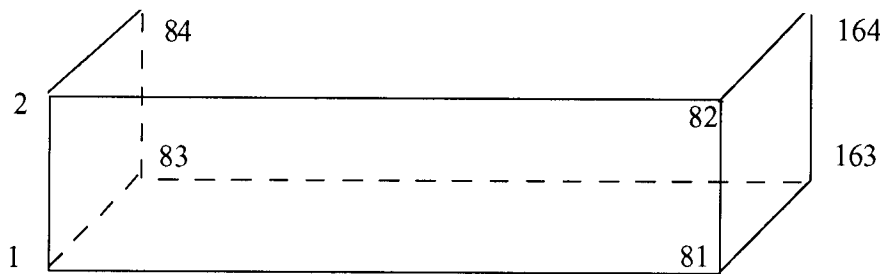


Figure 4.1 Schematic representation of the one-dimensional simulation domain.

Figure 4.2 shows the simulated breakthrough curves for CI at the end of the column for ten model trials described in Tables 4.1 and 4.2. The decrease in CI ion concentration over 160 hours occurs because TCE is being removed from the system by oxidation and the total mass in the system is decreasing.

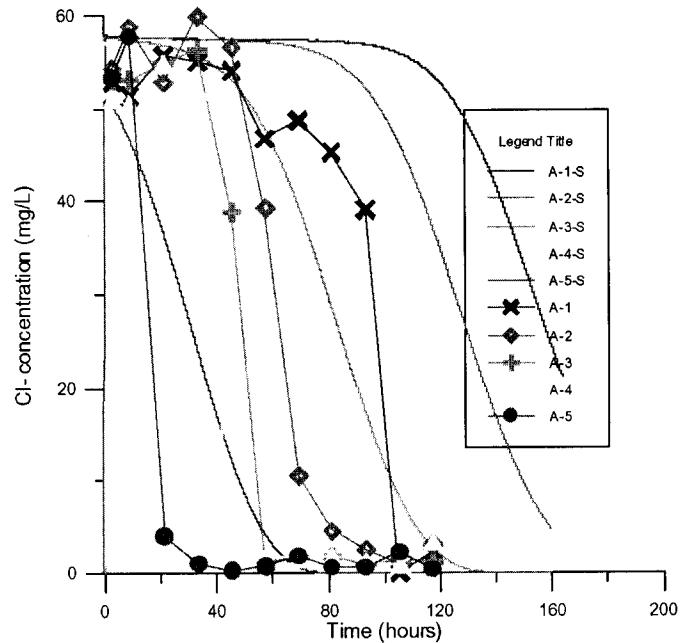


Figure 4.2 Decrease in Cl concentration as a function of time at the end of the column for ten simulated column experiments.

The accumulation of reaction products in the porous medium causes a reduction in both porosity and permeability. Figures 4.3 and 4.4 shows the variation in these parameters along the column after 160 hours. Generally, the pattern agrees generally with the experimental results, although more work is required on our part to more fully analyze these results. Most importantly, notice the greatest declines in porosity are associated with the greatest the declines in permeability. The maximum decrease in permeability is more than two-orders-of magnitude pointing to a severe restriction in the ability of the porous medium to transmit the oxidant.

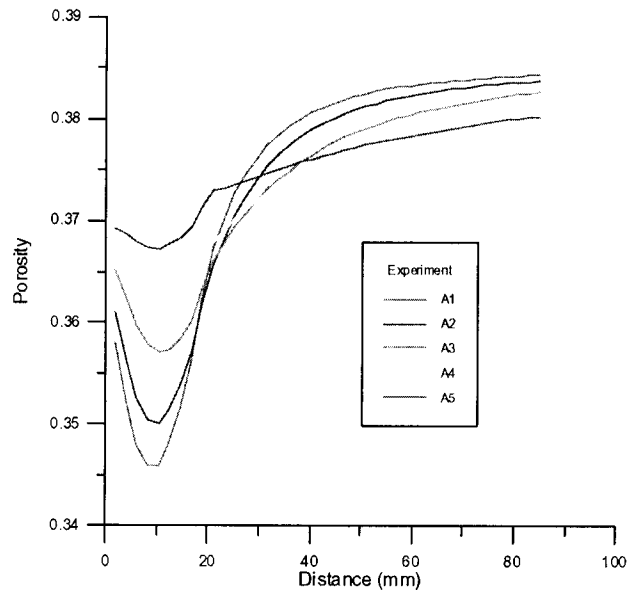


Figure 4.3 Change in porosity as a function of distance.

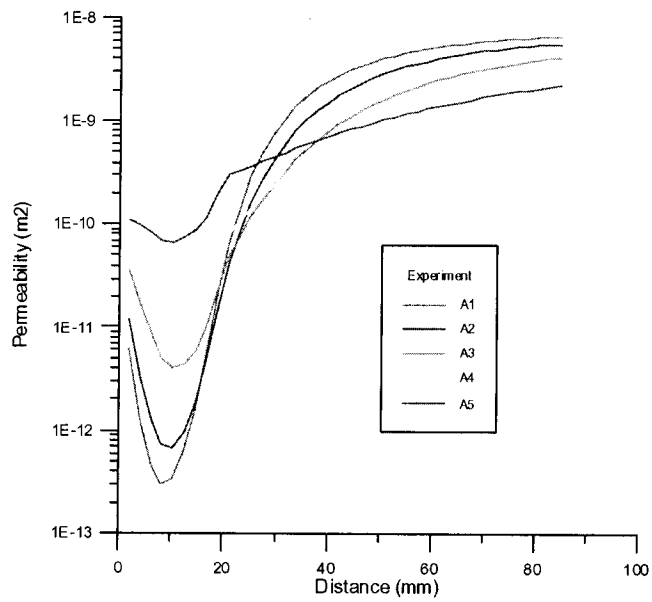


Figure 4.4 Change in permeability as a function of travel distance for the one-dimensional simulation trial.

Simulation of The Three-dimensional Tank Experiment

Preliminary results are available for a simulation trial that involved the large flow tank experiment discussed previously. At present, these results merely serve to illustrate how the code can be used for more complex problems. Given the very preliminary nature of these results, no analysis is possible at the present time.

Details describing the experiment and how it was run were presented in (Lee, et al., 2003). Figure 4.5 describes details of the model set up and especially the design of the grid. A TCE saturation of 0.08 was assigned to the source nodes. As before, the ends of the tank were constant flux and constant head boundaries. The other four sides were considered no flow boundaries.

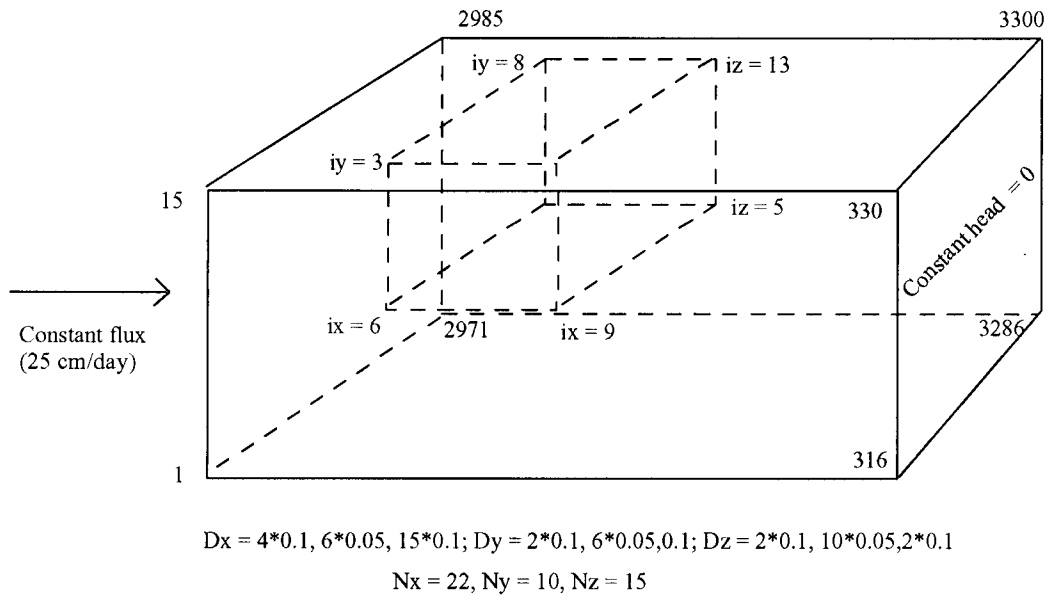


Figure 4.5 Schematic showing the design of the three-dimensional simulation experiment.

The simulations were run for 63 days, which corresponds to the actual length of the experiment. Figures 4.6, 4.7, and 4.8 illustrate the simulated distribution of TCE with time, the porosity and permeability, respectively. Qualitatively the results are quite comparable with the experiments, but additional work is required for further calibration and interpretation

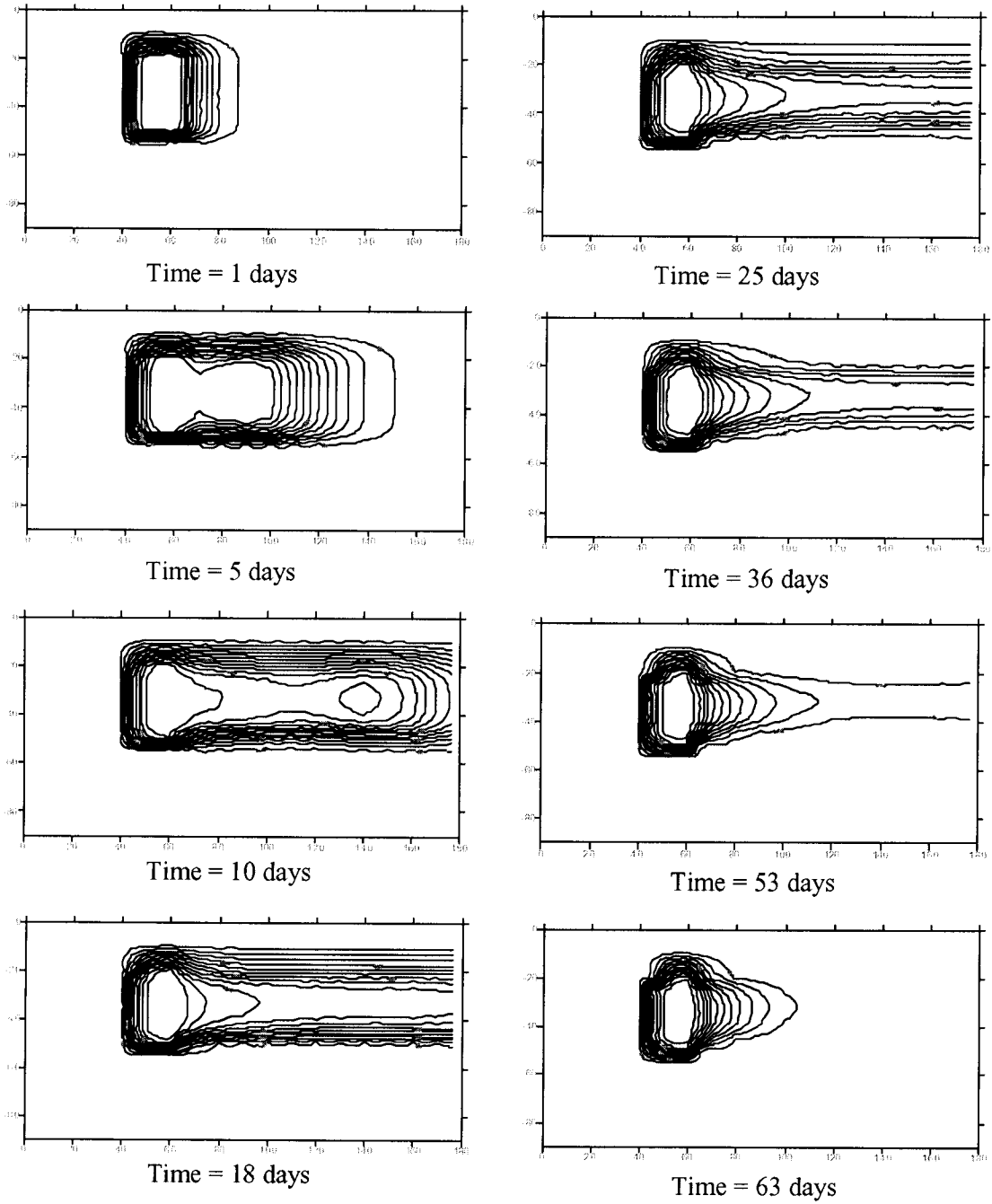


Figure 4.6 Time variation in the concentration of TCE in the porous medium.

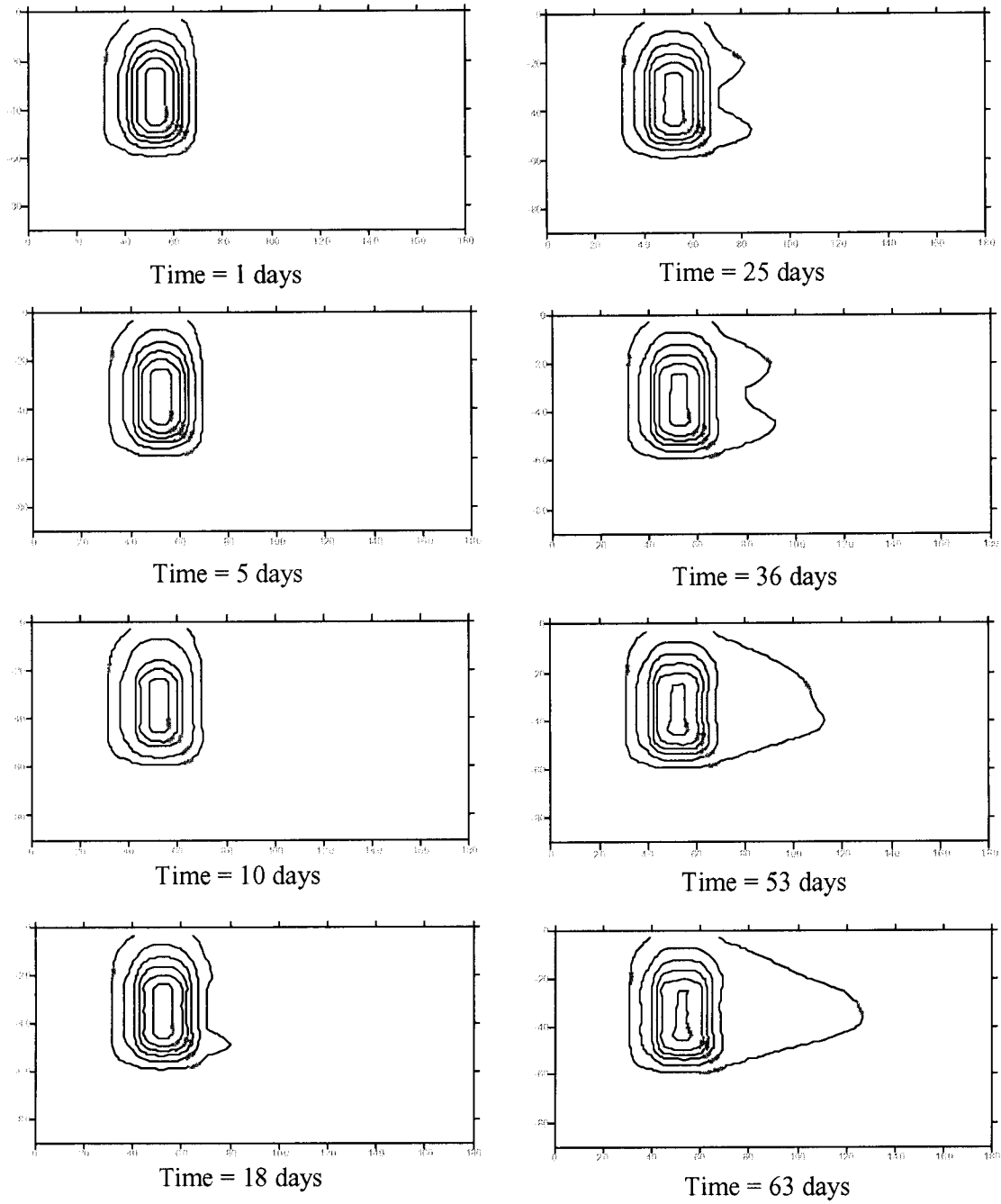


Figure 4.7 Porosity change as a function of space and time.

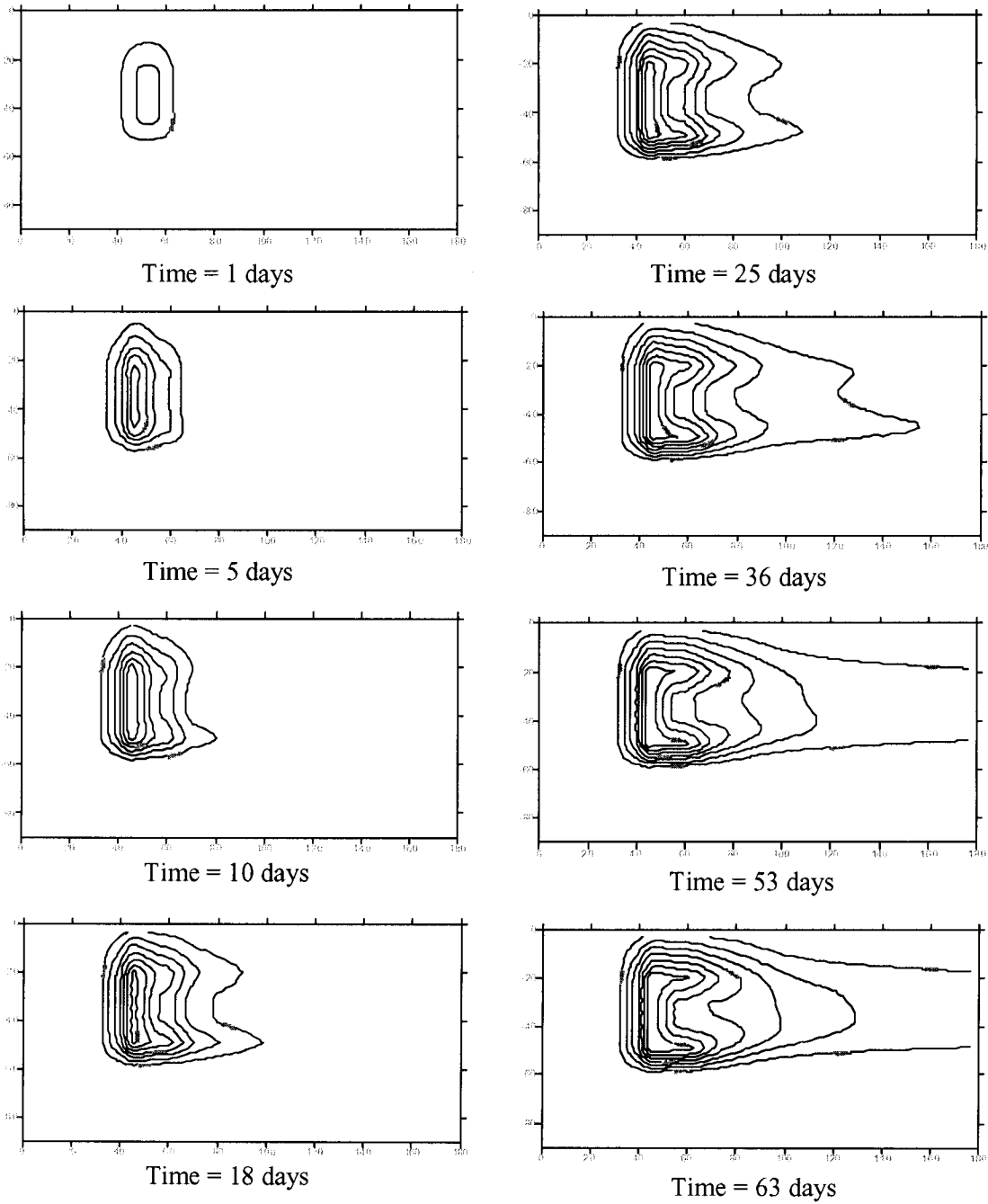


Figure 4.8 Permeability change as a function of space and time.

RELEVANCE, IMPACT AND TECHNOLOGY TRANSFER

The use of in situ oxidation approaches for the clean up of chlorinated solvents continues to be pursued actively for some types of spills. Now, as in the past, our research has been instrumental in elucidating the theoretical aspects and practical difficulties with this approach. The most important strategy for technology transfer remains with paper publication and oral presentations. As this report illustrates, we have been extremely active in this respect. We have been active in presenting at the Battelle DNAPL conference in Monterey, California, and various DOE conferences and workshops. Researchers and consultants that we talk with are aware of our research and papers, and it is clear that we are one of the worlds' leading research groups in this area.

We continue to assist individuals that call for information, sending out (mainly to consultants) copies of our papers and other work products. Now that a User's Guide is available for ISCO3D, we are able to share the code with interested scientists. Dr. Suresh Rao and students at Purdue are using the code for oxidation studies that they are conducting for SERDP. We are also exploring research opportunities in Korea.

PROJECT PRODUCTIVITY

We have gained significant understanding on fundamental scientific issues related to the in situ chemical oxidation with permanganate. We have also made several important progresses in helping put this technology into field practice. While developing the remediation techniques, we keep our research results updated with colleagues around the world. We have published our results on major academic journals and as book chapters. More than 10 conference presentations have been made at DOE workshops or other prominent national or international occasions. We have communicated with field scientists working at the remediation sites, and their responses are very helpful. We have collaborated with scientists in Japan and Korean which have helped promoting and marketing this technology

PERSONNEL SUPPORTED

Faculty:

Dr. Franklin W. Schwartz, Ohio Eminent Scholar in Hydrogeology

Post-Docs:

Dr. David Li

Dr. Yongkoo Seol

Dr. Eung Seok Lee

Graduate Student:

Yao-Chuen Fang

PUBLICATIONS

- Seol, Y., Schwartz, Frank W., Lee, S., 2001, Oxidation of binary DNAPL mixtures using potassium permanganate with a phase transfer catalyst. *Ground Water Monitoring and Remediation*, Spring 2001, p. 124-132.
- Li, X. D., and F. W. Schwartz, 2002. Permanganate oxidation schemes for the remediation of source zone DNAPLs and dissolved contaminant plumes, in *Chlorinated Solvents and DNAPL Remediation: Innovative Strategies for the Subsurface Cleanup*, edited by Henry, S. M., and Warner, S. D., Oxford University Press, pp. 73-85.
- Li, X. D., and F. W. Schwartz, 2003. DNAPL remediation with in situ chemical oxidation using potassium permanganate: I. Mineralogy of Mn oxide and its dissolution in organic acids, *Journal of Contaminant Hydrology*, In press.
- Li, X. D., and F. W. Schwartz, 2003. DNAPL remediation with in situ chemical oxidation using potassium permanganate: II. Increasing DNAPL removal efficiency by dissolving Mn oxide precipitates, *Journal of Contaminant Hydrology*. In press.
- Lee, E. S., Y. Seol, Y. C. Fang, and F. W. Schwartz, 2003. Destruction Efficiencies and Dynamics of Reaction Fronts Associated with the Permanganate Oxidation of Trichloroethylene, *Environmental Science and Technology*. 37 (11). p. 2540-2546.
- Seol, Y., F. W. Schwartz, and H. Zhang, 2003. A review of In Situ Chemical Oxidation and heterogeneity. *Environmental & Engineering Geoscience*, v. IX, No. 1, p. 37-50. Y.C.
- Fang, Y.C., R.A. Schincariol, F.W. Schwartz and Y. Seol, 2002. Multimedia Data Mining Applied to Site Investigation, Third International Conference on Remediation of Chlorinated and Recalcitrant Compounds, Monterey, CA, May 20-23, 2002.
- Li, X. D., and F. W. Schwartz, 2003. Use phosphate as inhibitor to control the Mn oxide colloid formation during the in situ chemical oxidation with permanganate, in *Remedial Science and Technology for Subsurface Contamination*, edited by Tiffany Zachry, Oxford University Press, submitted.

INTERACTIONS

Participation/Presentation at meeting, workshops, and conferences

- Li, X. David and Schwartz, Frank W., 2000, Chemical changes during the *in situ* permanganate treatment of chlorinated solvents in the subsurface, *Geological Society of American Annual Meeting*, Nov. 2000, Reno, NV.

- Li, X. David and Schwartz, Frank W., 2001, DNAPL source zone remediation by permanganate oxidation, DOE SCFA Midyear review conference, March 2001, Atlanta, GA.
- Seol, Y., F.W. Schwartz, M. Ibaraki, and X. Li, 2001. Permanganate treatment of dnapls in reactive barriers and source zone flooding schemes - permanganate oxidation in DNAPL source remediation. Poster Presentation EMSL PI Meeting. Hanford Washington.
- Li, X. David and Schwartz, F. W., 2001, Experimental test of a newly designed permanganate reactive barrier system for chlorinated solvents remediation. American Chemical Society Annual Meeting, April 2001, San Diego, CA.
- Lee, E. S., and F.W. Schwartz, 2002. Efficacy of strategies for the in situ oxidation of chlorinated solvents using potassium permanganate. Oral Presentation, Geological Society of America Meeting, Denver.
- Lee, E. S., and F.W. Schwartz, 2002. Semi-passive, long-term treatment of DNAPL using slow-release KMnO_4 , December 2002, Yonsei University, Korea.
- Lee, E. S., and F.W. Schwartz, 2002. Semi-passive, long-term treatment of DNAPL using slow-release KMnO_4 , December 2002, Korea Agricultural and Rural Infrastructure Corporation, Korea.
- Li, X. David and Schwartz, F. W., 2003. In Situ Chemical Oxidation for the Remediation of Ground Water and Soil Contaminated by Chlorinated Organic Solvents. Department of Geology and Geophysics, University of New Orleans, New Orleans, LA. March 2003.
- Lee, E. S., and F.W. Schwartz, 2003. Slow-release permanganate and its applications to groundwater remediation, November 2003, GSA Annul Meeting, Seattle, WA.
- Lee, E. S., and F.W. Schwartz, 2003. Semi-passive, in situ chemical oxidation scheme using slow-release KMnO_4 , Yonsei University, August 2003, Korea.
- Schwartz, F. W., E. S. Lee, and David X. Li, Permanganate treatment of DNAPLs in reactive barriers and source zone flooding schemes, May 2003, EMSP Workshop, Richland, WA
- Li, X. David and Schwartz, F. W., 2003. Schemes for the treatment of Mn oxide precipitation during in situ chemical oxidation using permanganate. 225th National Meeting of American Chemical Society, New Orleans, LA, March 2003.

LITERATURE CITED

- Ahfeld, D.P., Dahmani, A., and Ji, W., 1994, A conceptual model of field behavior of air sparging and its implications for application. *Ground Water Mon. Rev.*, Vol 14(3), pp. 132-139.
- Conrad, S. H., Glass, R. J., and Peplinski, W. J., 2002, Bench-scale visualization experiments of DNAPL remediation processes in analog heterogeneous aquifers; surfactant floods and in-situ oxidation using permanganate. *Journal of Contaminant Hydrology*, 58 (1-2): 13-49.
- Ibaraki, M. and Schwartz, F. W. 2001, Efficiency of chemical floods for the in-situ treatment of DNAPL source zones: *Ground Water*, 39(5), 660-666.
- Lee, E.S. Seol, Y. Fang, Y. C., and Schwartz, F. W., 2003. Destruction efficiencies and dynamics of reaction fronts associated with the permanganate oxidation of trichloroethylene. *Environmental Science and Technology*, 37, 13, 2913-2919.
- Li, X. and Schwartz, F. W., 2000, Efficiency problems related to permanganate oxidation schemes, in *The Second International Conference on Remediation of Chlorinated and Recalcitrant Compounds*, Vol. C2-6: Chemical Oxidation and Reaction Barriers, Monterey, CA, pp. 41-48.
- Reis, J.C. and Acock, A.M. 1994. Permeability reduction models for the precipitation of inorganic solids in Berea sandstone. *In Situ*, 18, 3, 347-368.
- Reitsma, S. and Marshal, M. In *Treating dense nonaqueous-phase liquids (DNAPLs): Remediation of chlorinated and recalcitrant compounds*; Wickramanayake, G.B., Gavaskar, A.R., Gupta, N., Ed. 2000, Battelle Press, Columbus, OH, pp 25-32.
- Seol, Y., F. W. Schwartz, and H. Zhang, 2002. A review of In Situ Chemical Oxidation and heterogeneity. *Environmental & Engineering Geoscience*, v. IX, No. 1, p. 37-50.
- Schnarr, M., Truax, C., Farquhar, G., Hood, E., Gonullu, T., and Stickney, B., 1998. Laboratory and controlled field experiments using potassium permanganate to remediate trichloroethylene and perchloroethylene DNAPLs in porous media. *Journal of Contaminant Hydrology*, 29, 205-224.

- Schroth, M.H., Oostrom, M., Wietsma, T.W., and Istok, J.D. In-situ oxidation of trichloroethene by permanganate: effects on porous medium hydraulic properties. *Journal of Contaminant Hydrology*, 2001, 50, 79-98.
- Zhang, H., and Schwartz, F. W., 2000a, Simulation of oxidative treatment of chlorinated compounds by permanganate. In *Chemical Oxidation and Reactive Barriers: Remediation of Chlorinated and Recalcitrant Compounds*, Wickramanayake, G. B., Gavaskar, A. R., and Chen, A. S. C. (Editors), 2000, Battelle Press, Columbus, OH. p 1-8.
- Zhang, H. and F. W. Schwartz, 2000b, Simulating the in situ oxidative treatment of chlorinated ethylenes by potassium permanganate. *Water Resource Research*. 36(1), 3031-3042.
- West, O. R., S. R. Cline, W. L. Holden, F. G. Gardner, B. M. Schlosser, J. E. Thate, D. A. Pickering, T. C. Houk, A full-scale demonstration of in situ chemical oxidation through recirculation at the X-701B site, Oak Ridge National Laboratory, Oak Ridge, TN, ORNL/TM-13556, 101 p., 1997.